Journal of Pharmaceutical Sciences 105 (2016) 3256-3268

Contents lists available at ScienceDirect

Journal of Pharmaceutical Sciences

journal homepage: www.jpharmsci.org

Drug Discovery—Development Interface

Determination of the Degradation Chemistry of the Antitumor Agent Pemetrexed Disodium

Patrick J. Jansen [1,*], William K. Smith [1], Steven W. Baertschi [2], Douglas E. Dorman [1], Craig A.J. Kemp [1], Karen A. McCune [1]

[1] Lilly Research Laboratories, Eli Lilly and Company, Indianapolis, Indiana 46285
[2] Baertschi Consulting, Carmel, Indiana 46033

ARTICLE INFO

Article history:
Received 31 March 2016
Revised 31 May 2016
Accepted 7 June 2016
Available online 15 August 2016

Keywords:
chemical stability
degradation products
LC-MS
oxidation
photodegradation
stability

ABSTRACT

Stress-testing (forced degradation) studies have been conducted on pemetrexed disodium heptahydrate (**1**) (LY231514·2Na·7H_2O) drug substance in order to identify its likely degradation products and establish its degradation pathways. Solid samples of the drug substance were stressed under various conditions of heat, humidity, and light, and solutions of the drug substance were stressed under various conditions of heat, light, oxidation, and over a wide pH range (1-13). The stressed samples were analyzed using a gradient elution reversed-phase HPLC method. The 7 major degradation products detected in the stress-testing studies were isolated, and the structures were elucidated via spectroscopic characterization. The structures of the degradation products and their proposed mechanisms of formation indicate that **1** degrades *via* 2 main pathways: oxidation and hydrolysis. Of the 7 identified degradation products, 6 are proposed to result from oxidation and 1 from hydrolysis.

Introduction

Pemetrexed disodium heptahydrate (**1**) (LY231514·2Na·7H_2O) is the active ingredient in Alimta®, a folate analog metabolic inhibitor. Alimta is formulated as a lyophilized cake that is reconstituted prior to administration. Degradation studies have been conducted on the heptahydrate form of **1** as well as the corresponding 2.5 hydrate in order to gain an understanding of the degradation chemistry of **1**. A review of the literature indicates that abbreviated degradation studies have been conducted on **1** by others in support of method development, but these degradation studies are largely incomplete in that they do not provide the structures of degradation products nor do they discuss the degradation mechanism(s).[1-4] One literature article mentions glutamic acid and des-glutamate (**7**) as potential degradation products but makes no mention of any other degradation products.[5] More recently, Warner et al.[6] discussed the development of a purity control strategy and the associated analytical methodology, providing structures of the major degradation products but providing no discussion of structure elucidation or degradation pathways.

The degradation studies described herein consist of stress-testing (forced degradation) experiments to generate potential degradation products and to determine the conditions under which **1** degrades. The stress-testing studies included exposure of **1** to a wide variety of stress conditions in both the solid state and in solution. Solid samples of **1** were stressed under various conditions of heat, humidity, and light while solutions of **1** were stressed under various conditions of heat, light, oxidation, and over a wide pH range (1-13) per International Council for Harmonization (ICH) Q1A and Q1B recommendations.[7] Stressed samples were analyzed for loss of parent and degradation product increases using reversed-phase HPLC with UV-photodiode array detection. The major degradation products detected in the stress testing studies were isolated with preparative chromatography and characterized using mass spectrometry, 1 and 2-D ^{1}H nuclear magnetic resonance (NMR), and ^{13}C NMR. The major degradation products detected in the stress-testing studies are potential degradation products that were used to develop the stability-indicating control methods. Stability studies conducted on samples of the heptahydrate of **1** indicate that it is stable and does not undergo degradation when packaged appropriately. Stability studies conducted on the lyophilized formulation of **1** also indicate that it is stable when packaged in vials with a nitrogen overlay to minimize the level of oxygen.

* *Correspondence to:* Patrick J. Jansen (Telephone: +1 317 292-0550).
E-mail address: patjansen@lilly.com (P.J. Jansen).

http://dx.doi.org/10.1016/j.xphs.2016.06.029
0022-3549/

Experimental

Solid-State Stress

Solid-state samples of either **1** or the 2.5 hydrate were exposed to conditions of heat and humidity. Thermally stressed samples were generated by storing samples in an oven at 70°C under either uncontrolled or high humidity (~75% relative humidity [RH]) conditions. The high-humidity condition was achieved by storing the samples in a small open container which was enclosed in a larger container containing a saturated sodium chloride solution. All of the initial stress-testing work was conducted on the 2.5 hydrate since that was the polymorph form of the drug substance being developed at the time the stress-testing studies were carried out. X-ray powder diffraction and solid-state NMR confirmed that no changes in crystal form were observed in samples stored under uncontrolled humidity at either 40°C or 70°C. The samples stored under high humidity at either 40°C or 70°C, however, changed crystal form to the heptahydrate (**1**). Consequently, both the 2.5 hydrate and heptahydrate forms have been thermally stressed. Photostressed samples were generated by exposing a thin layer of the 2.5 hydrate of **1** (<1-mm thickness) to either simulated sunlight generated by a xenon arc lamp or fluorescent light produced by a bank of 8 cool white fluorescent tubes in an enclosed box. Refer to Table 1 for the solid state stress results.

Solution Stress

The hydrolytic stability of **1** was investigated by preparing solutions at a concentration of approximately 0.8 mg/mL as the free acid in the following solvents and stressing at 70°C: (1) 0.1-N HCl/acetonitrile 75/25, (2) 25-mM sodium phosphate titrated to pH 2/acetonitrile 75/25, (3) 25-mM sodium phosphate titrated to pH 4/acetonitrile 75/25, (4) 25-mM sodium phosphate titrated to pH 6, (5) 25-mM sodium phosphate titrated to pH 8, (6) 0.1-N NaOH, and (7) water. Samples for analysis were taken at 1, 3, and 7 days. The photostability of **1** was investigated by preparing solutions in water at a concentration of approximately 1 mg/mL and exposing to either simulated sunlight or fluorescent light. The oxidative susceptibility of **1** was investigated by preparing solutions in either 0.3% hydrogen peroxide or in 20/80 (vol/vol) water/acetonitrile containing the radical initiator 2,2'-azobisisobutyronitrile at a concentration of 1 mg/mL. All solutions were diluted 5-fold with 25-mM phosphate titrated to pH 2.5/acetonitrile (75/25) prior to HPLC assay. Refer to Table 2 for the solution stress results.

Photostability Chambers

The photostability chamber was a Suntest CPS$^+$ manufactured by Atlas Material Testing Solutions (Chicago, IL). It was set up to simulate natural sunlight and contained a xenon long-arc lamp with an infrared filter and a UV filter with a cutoff of 300 nm. The black standard temperature was set at 30°C, and the chamber reached a temperature of 27°C during exposure. Foil-wrapped samples were placed alongside during light exposure as controls. The photostability chamber was set at an intensity of 765 W/m^2 (300-800 nm). Manufacturer measurements indicate that this setting corresponds to a visible intensity of ~150,000 lux, and a UVA intensity (320-400 nm) of 78 W/m^2. Thus, a 10-h sample exposure corresponds to ~1.5 million lux-h visible and ~780 W-h/m^2 UVA. For comparison, the ICH guideline on photostability[7] specifies a minimum exposure of 1.2 million lux-h in the visible and not less than 200 W-h/m^2 in the near UV for confirmatory studies.

The fluorescent light chamber consisted of 8 Sylvania Cool White Supersaver T8/F32/SP41 fluorescent tubes in a 19″ × 50″ box. The visible intensity of the light was approximately 17,000 lux at the level of the samples. The chamber was ventilated with a fan and maintained an average temperature of approximately 26°C.

Analytical HPLC Method

HPLC analyses were carried out on a Waters photodiode array system consisting of a 600E controller and pump, a 715 Ultra Wisp, and a 996 photodiode array detector. The column, a 4.6 × 150 mm Zorbax SB-C_8, 3.5 μm (MAC-MOD Analytical), was operated at 30°C. The flow rate was maintained at 1.0 mL/min. Mobile phases A and B consisted of 97/3 and 30/70 (vol/vol) 25-mM NaH_2PO_4 (pH adjusted to 2.5 with H_3PO_4)/acetonitrile, respectively. Mobile phase B was increased linearly from 0% to 18% at 1.8% per minute for 10 minutes, held at 18% for 12 minutes, and then increased linearly from 18% to

Table 1
Solid-State Stress Test Results

Storage Condition	Polymorph Form	Time	Assay (% Initial)	Impurity Increase (%)	Physical Appearance (Color)	Degradation Products Observed
40°C/uncontrolled RH	LY231514·2Na·2H_2O	28 d	99.8	0.5	Off-white	**2**
		56 d	100.0	1.2	Off-white	
40°C/75% RH	LY231514·2Na·2H_2O	28 d	101.1	0.0	Off-white	None
	that converted to LY231514·2Na·7H_2O	56 d	101.6	0.2	Off-white	
70°C/uncontrolled RH	LY231514·2Na·2H_2O	14 d	97.7	2.2	Off-white	**3, 4, 5**
		28 d	94.0	4.2	Light tan	
70°C/75% RH	LY231514·2Na·2H_2O	14 d	79.9	13.6	Green	**3, 4, 5**
	that converted to LY231514·2Na·7H_2O	28 d	85.8	9.5	Green	
Simulated sunlight	LY231514·2Na·2H_2O	10 h	94.8	1.8	Tan	**5, 6**
		20 h	95.0	1.9	Tan	
Simulated sunlight (wrapped control)	LY231514·2Na·2H_2O	10 h	100.0	0.1	Off-white	None
		20 h	100.3	0.3	Off-white	
Fluorescent light, 17,000 lux, 27°C	LY231514·2Na·2H_2O	7 d	97.4	1.6	Off-white	**5, 6**
		14 d	97.1	1.9	Off-white	
		28 d	95.4	2.4	Tan	
~Fluorescent light, 17,000 lux, 27°C (wrapped control)	LY231514·2Na·2H_2O	7 d	99.4	0.4	Off-white	None
		14 d	100.2	0.3	Off-white	
		28 d	101.0	0.4	Off-white	
Simulated sunlight	LY231514·2Na·7H_2O	20 h	97.2	1.1	Tan	**5, 6**
Simulated sunlight (wrapped control)	LY231514·2Na·7H_2O	20 h	98.5	0.0	Off-white	None

Table 2
Solution Stress Test Results

Storage Condition	Time	Assay (% Initial)	Impurity Increase (%)	Physical Appearance (Color)	Degradation Products Observed
Solution in H_2O at 70°C	3 d	99.1	3.9	Colorless	**3, 4**
	7 d	94.8	7.8	Colorless	
	14 d	86.9	15.1	Pale yellow	
Solution in 25/75 (vol/vol) ACN/ 0.1-N HCl at 70°C	1 d	94.4	5.3	Pale green	**3, 4, 6, 7**
	2 d	89.3	10.0	Pale green	
	3 d	84.8	13.3	Pale green	
Solution in 25/75 (vol/vol) ACN/ pH 2 buffer at 70°C	1 d	96.9	3.1	Pale green	**3, 4, 6, 7**
	2 d	92.6	5.9	Pale green	
	3 d	88.6	8.4	Pale green	
Solution in 25/75 (vol/vol) ACN/ pH 4 buffer at 70°C	3 d	97.4	1.9	Pale yellow	**3, 6**
	7 d	96.0	4.1	Pale yellow	
	14 d	90.2	8.3	Yellow	
Solution in pH 6 buffer at 70°C	3 d	99.8	3.4	Colorless	**3, 4**
	7 d	95.4	7.2	Pale yellow	
	14 d	86.4	14.1	Pale yellow	
Solution in pH 8 buffer at 70°C	3 d	92.9	4.8	Pale yellow	**3, 4**
	7 d	87.4	10.6	Pale yellow	
	14 d	74.7	20.6	Pale yellow	
Solution in 0.1-N NaOH at 40°C	1 d	93.3	4.2	Pale yellow	**3, 4, 8**
	3 d	83.3	13.2	Yellow	
	7 d	69.7	25.7	Yellow	
Solution in H_2O exposed to simulated sunlight	2 h	85.2	8.7	Yellow	**3, 4, 5, 6**
	4 h	63.9	19.8	Yellow	
	6 h	39.0	31.8	Yellow	
Solution in H_2O exposed to simulated sunlight (wrapped control)	6 h	99.6	0.3	Colorless	None
Solution in H_2O exposed to fluorescent light at intensity of 1000 lux	14 d	103.0	0.6	Colorless	**3**
	28 d	101.2	1.5	Colorless	
	56 d	98.1	4.4	Pale yellow	
Solution in H_2O exposed to fluorescent light at intensity of 1000 lux (wrapped control)	14 d	102.9	0.3	Colorless	**3**
	28 d	103.3	1.1	Colorless	
	56 d	99.7	1.7	Colorless	
Solution in 0.3% H_2O_2, ambient temperature	1 d	97.6	3.8	Colorless	**3, 6**
	3 d	90.5	9.7	Colorless	
	7 d	78.2	19.6	Colorless	
Solution in 80/20 (vol/vol) ACN/ H_2O at 40°C containing the radical initiator AIBN	1 d	87.9	9.2	Pale yellow	**3, 6**
	3 d	72.0	23.1	Yellow	
	7 d	46.7	47.8	Yellow	
Solution in 80/20 (vol/vol) ACN/ H_2O at 40°C	1 d	100.2	0.1	Colorless	None
	3 d	98.0	0.3	Colorless	
	7 d	100.1	0.4	Colorless	

100% at 8.2% per minute for 10 minutes. Chromatograms were extracted at 228 nm and the levels of degradation products measured by dividing their area by the total area of all peaks. The method was shown to give a linear response for **1** over the concentration range used in the studies. The limit of quantitation for degradation products was estimated to be approximately 0.01% indicating that the method is easily able to detect degradation products at the 0.1% level.

Generation of Degradation Products for Isolation

The oxidative dimers (**3**) and ring-opened ketoamine **(4)** were generated by continuously purging an aqueous solution of **1** (5 mg/mL) and sodium bisulfite (1.6 mg/mL) with air for 64 hours (prior experiments had determined that bisulfite catalyzes the degradation of **1** in solution). HPLC analysis of this solution revealed the presence of ~20% oxidative dimers (**3**) and ~6% ring-opened ketoamine **(4)** as well as a bisulfite adduct of **1**. Both degradation products (**3** and **4**) were isolated from the mixture using reversed-phase preparative HPLC (method A) and the solvent removed by lyophilization. The α-hydroxy lactams **(8)** were generated by reacting **1** with singlet oxygen generated by irradiating an aqueous solution of the photosensitizer rose bengal and **1** with intense fluorescent light (~17,000 lux) for 3 hours. Prior experiments indicated that exposure of **1** to singlet oxygen rapidly generates the α-hydroxy lactams **(8)**. The α-hydroxy lactams were isolated from this solution using reversed-phase preparative HPLC (method B) and the solvent removed by lyophilization. Prior to lyophilization, the pH of the isolated fraction was raised to approximately pH 7 with ammonium hydroxide to eliminate dehydration of the α-hydroxy lactams **(8)** to a mixture of E and Z enones during the lyophilization process. The lactams **(6)** were generated using the radical initiator 2,2'-azobis(2,4-dimethylvaleronitrile). A solution containing **1** and the radical initiator both at a concentration of approximately 1 mg/mL in 80/20 (vol/vol) acetonitrile/water was held at 40°C for 21 hours and 55°C for 2 hours. The lactams **(6)** were isolated from the mixture using reversed-phase preparative HPLC (method A) and the solvent removed by lyophilization. The ring-opened ketoformamide **(5)** and epoxy hemiaminal **(2)** were generated by heating the 2.5 hydrate of LY231514 at 70°C for 52 days. Both degradation products were isolated from the mixture using reversed-phase preparative HPLC (method A) and the solvent removed by lyophilization. The des-glutamate **(7)** was not isolated because its structure was verified by comparing its retention time and UV spectrum to authentic synthesized material.

Preparative HPLC Methods

The preparative separations were carried out on a Varian preparative system consisting of 2 Model SD-1 pumps, a Dynamax Model UV-1 variable wavelength detector set at 260 nm, and a Dynamax

Model FC-1 fraction collector. Both preparative methods utilized a 50.8 × 250 mm Kromasil 100-10C18, 10-μm column (Technikrom) operated at ambient temperature with a flow rate of 70 mL/min. For method A, mobile phases A and B consisted of 0.1% trifluoroacetic acid in water and 0.1% trifluoroacetic acid in acetonitrile (vol/vol), respectively. Mobile phase B was held constant at 20% for a total run time of 20 min. For method B, mobile phases A and B consisted of 0.2% acetic acid in water and acetonitrile (vol/vol), respectively. Mobile phase B was increased linearly from 3% to 40% at a rate of 1.23% per min.

High Resolution Mass Spectrometry

High-resolution positive-ion electrospray (ES^+) spectra were obtained by liquid chromatography—mass spectrometry using an Agilent 6230 time-of-flight spectrometer coupled to an Agilent 1200 LC system. The system was controlled and data manipulated with Agilent MassHunter software.

NMR

Proton and carbon-13 NMR spectra were recorded at 299.957 and 75.432 MHz, respectively, using a Varian Unity spectrometer equipped with a 5-mm Nalorac indirect detection probe and a Matrix™ shim system. Samples consisted of 21 mg/mL of **2**, 30.1 mg/mL of **3**, 11.7 mg/mL of **4**, 25 mg/mL of **5**, and 46.6 mg/mL of **6** dissolved in dimethylsulfoxide-d_6. A sample of **8** was prepared at a concentration of 42.7 mg/mL in D_2O. Chemical shifts are reported in parts per million relative to dimethylsulfoxide-d_6 (2.50 ppm ^1H, 39.50 ^{13}C) or D_2O (4.79 ppm). All spectra were recorded in a nonspinning mode.

Results and Discussion

Analytical Method Development

The reversed-phase HPLC method was designed to maximize the probability of resolving degradation product peaks from the parent peak and detecting degradation products possessing significantly different polarity than **1**. A multistep gradient elution was chosen to maximize resolution and to cover a wide polarity range. The first segment of the gradient starts at very low organic concentration and ramps to an organic concentration in which **1** is eluted under essentially isocratic conditions. The third segment of the gradient begins after the **1** elutes and is a rapid ramp to high organic concentration to elute any nonpolar degradation products.

Solid-State Stress Testing

Stress testing of solid samples of **1** was conducted at either 40°C or 70°C at both low (uncontrolled) and high humidity (75% RH). Representative chromatograms obtained on these samples are shown in Figure 1. At 70°C both the degradation rate and degradation profile of **1** are dependent upon humidity, with the rate of degradation significantly faster at high humidity. At 40°C, the degradation of **1** is significantly slower and the humidity dependence is minor. All of the degradation products formed under thermal conditions are proposed to result via an oxidative mechanism, indicating that **1** is susceptible to oxidative degradation as a solid.

Photodegradation studies were conducted on solid-state samples of **1** using either fluorescent light or simulated sunlight generated using ICH Q1B, option 1 conditions (xenon arc lamp). Representative chromatograms obtained on these samples are shown in Figure 2. The results obtained indicate slight photoinstability in the solid state when exposed to cool-white fluorescent light photostress for 14 days (~11 million lux-h total dose) or simulated sunlight photostress for 20 h (~3 million lux-h visible and ~1560 W-h/m^2 near UV total dose). Additionally, some color change of the drug substance from an initial off-white color to tan was observed upon exposure to simulated sunlight for 20 h.

Solution Stress Testing

The stability of **1** in solution was investigated from pH 1 (0.1-N HCl) to pH 13 (0.1-N NaOH). Since **1** is not soluble to an appreciable extent in totally aqueous solutions at low pH, a cosolvent (acetonitrile) was added to the solutions at pH 4 and lower to obtain complete dissolution. Representative chromatograms obtained on the solution samples are shown in Figures 3 and 4. Hydrolysis of **1**

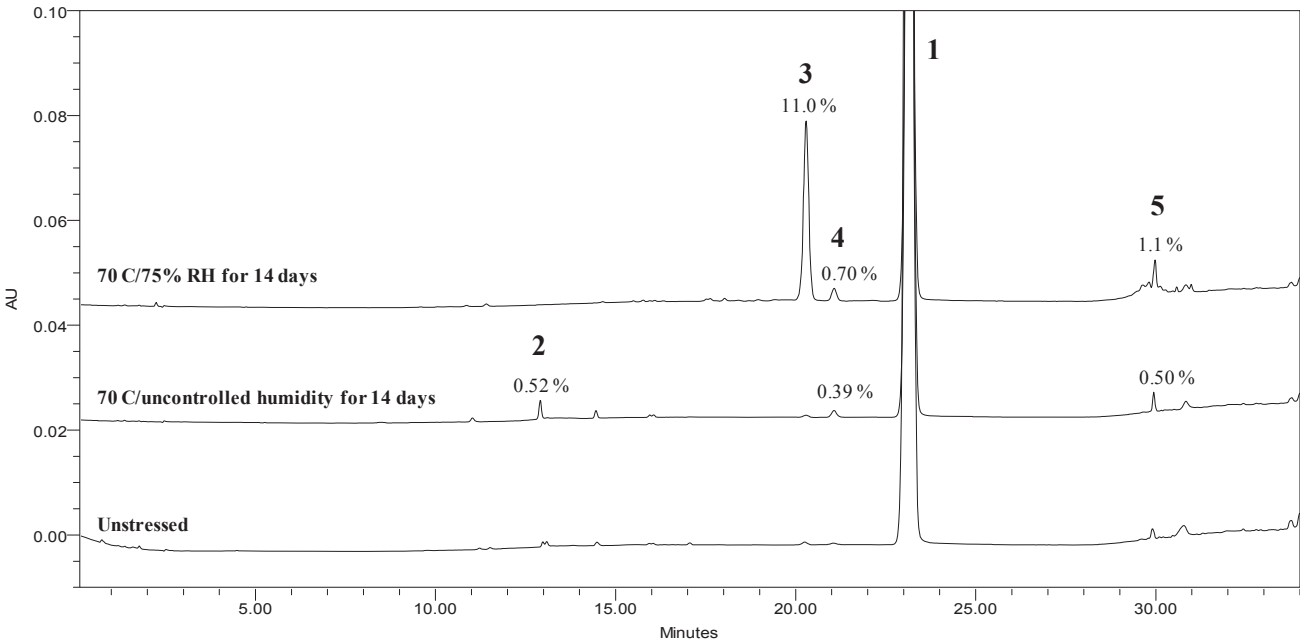

Figure 1. HPLC chromatograms obtained on thermally stressed solid-state samples of **1**.

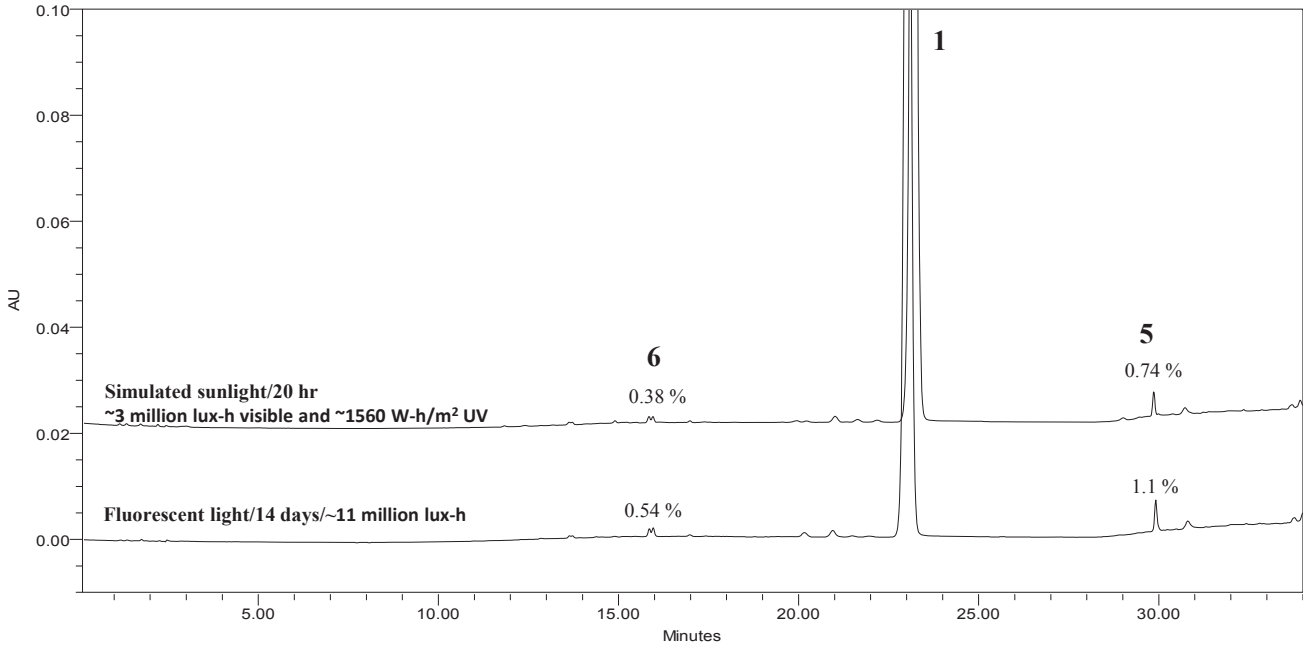

Figure 2. HPLC chromatograms obtained on photostressed solid-state samples of **1**.

to the des-glutamate (**7**) was the dominant degradation mechanism at low pH (pH 1 and pH 2). As the pH was raised to 4 and greater, oxidation became the dominant degradation mechanism, with the oxidative dimers (**3**) being the major degradation products detected under these conditions.

The susceptibility of aqueous solutions of **1** to peroxide-mediated degradation and free radical–induced degradation was studied by preparing solutions of **1** containing either dilute (0.3%) hydrogen peroxide or the radical initiator 2,2'-azobisisobutyronitrile. Refer to Figure 5 for the chromatograms. Both of these solutions exhibited significant degradation to the oxidative dimers (**3**) and lactams (**6**), suggesting that **1** is susceptible to both free radical and peroxide-mediated degradation.

The photostability of **1** in water was assessed by exposing solutions to either ambient lab lighting (cool white fluorescent light at an intensity of 1000 lux for 28 days, ~672,000 lux-h total dose) or simulated sunlight (10 h at an intensity of ~150,000 lux and ~78 W/m^2, ~1.5 million lux-h visible and ~780 W-h/m^2 near UV). The solution exposed to simulated sunlight underwent significant degradation, giving rise to a number of degradation products resulting from oxidation of **1**. When compared to a foil-wrapped control sample, the solution exposed to fluorescent light for 28

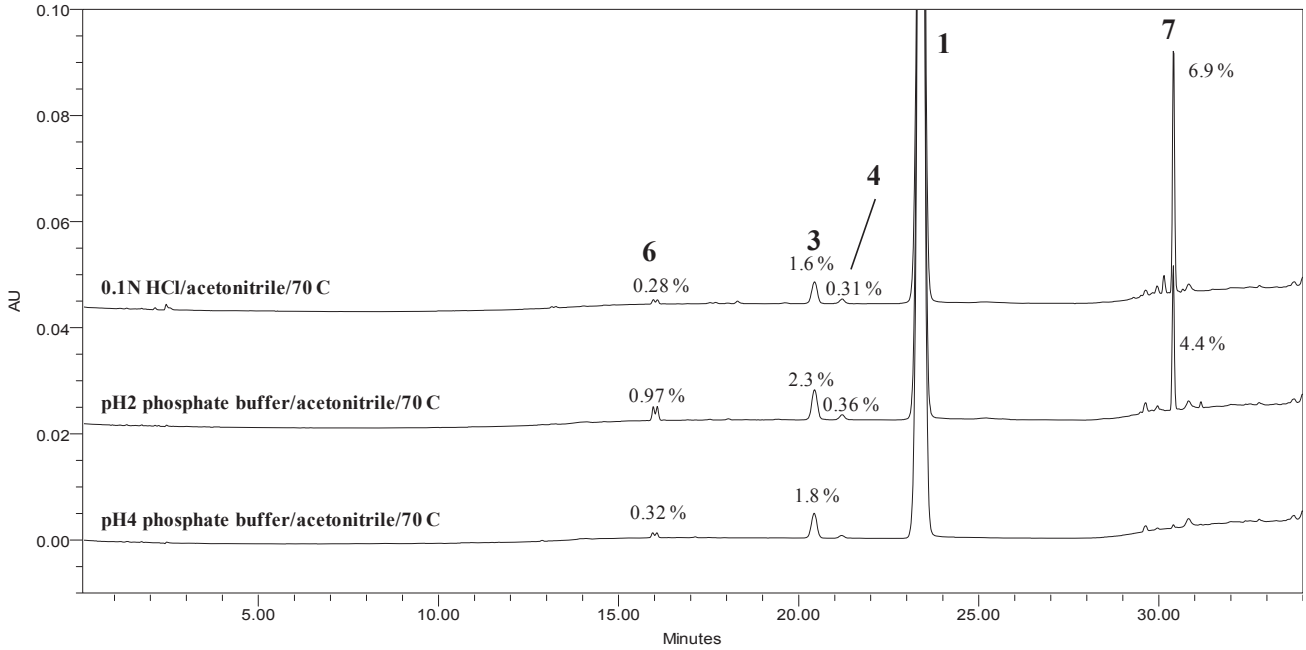

Figure 3. HPLC chromatograms obtained on solutions of **1** stressed at 70°C for 3 days.

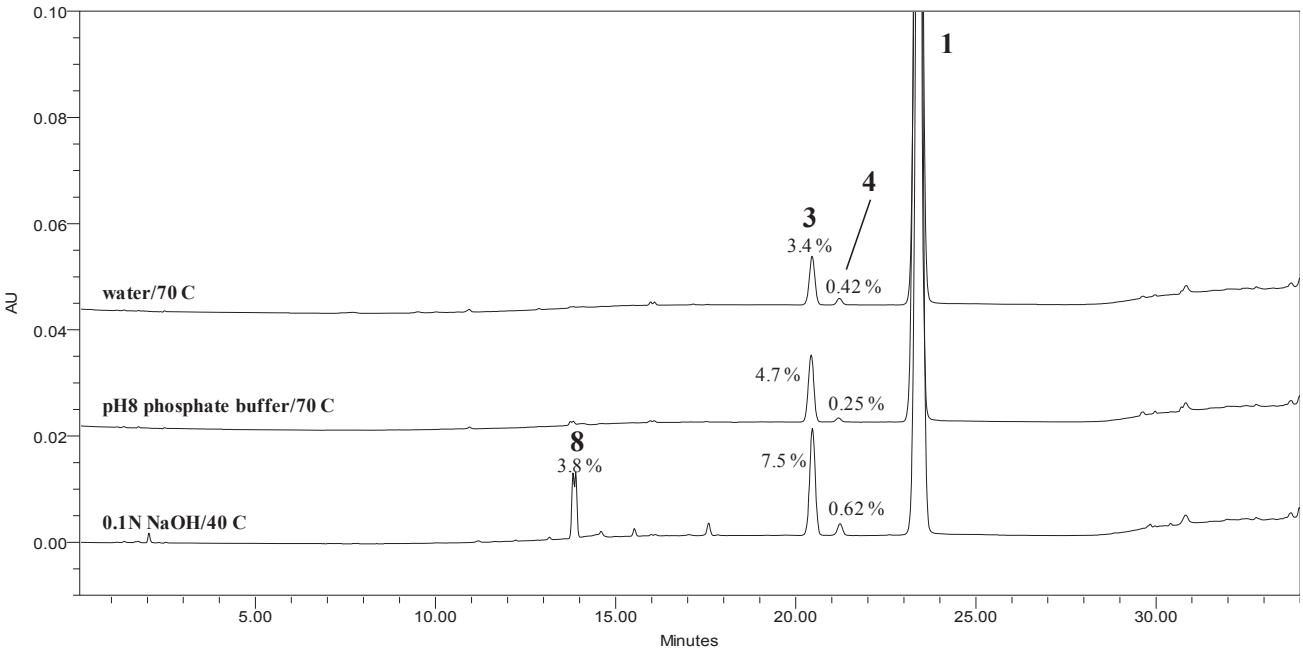

Figure 4. HPLC chromatograms obtained on solutions of **1** stressed for 3 days at 70°C.

days exhibited only minor (~0.5 %) degradation. Refer to Figure 6 for the chromatograms. The solution photostability results indicate that short-term (i.e., a few days) exposure of solutions of **1** to typical indoor lighting will not result in significant degradation of **1**.

Characterization of Degradation Products

Des-glutamate (**7**)—the late-eluting des-glutamate degradation product (**7**) was readily identified by comparison of its UV spectrum and HPLC retention time to that of synthesized material. The remaining degradation products did not match the known related compounds of **1** and so were isolated and characterized using NMR and MS.

Epoxy hemiaminal (**2**)—the high-resolution ES^+ measurements on the epoxy hemiaminal (**2**) indicated an *m/z* value of 460.1470 for the protonated molecular ion. This mass corresponds to a formula of $C_{20}H_{22}N_5O_8$ (theoretical mass 460.1463, 1.5 ppm error) and indicates a molecular formula of $C_{20}H_{21}N_5O_8$ for **2**. This formula corresponds to the addition of 2 oxygen atoms to **1**. The NMR characterization of the epoxy hemiaminal **(2)** was challenging due to the instability of the compound. Examination of the proton and carbon NMR spectra indicates that the modifications of **1** leading to the epoxy hemiaminal **(2)** have all occurred on the pyrrolopyrimidone portion of the molecule. Careful analysis of the full NMR data set leads to the proposed structure of the epoxy hemiaminal

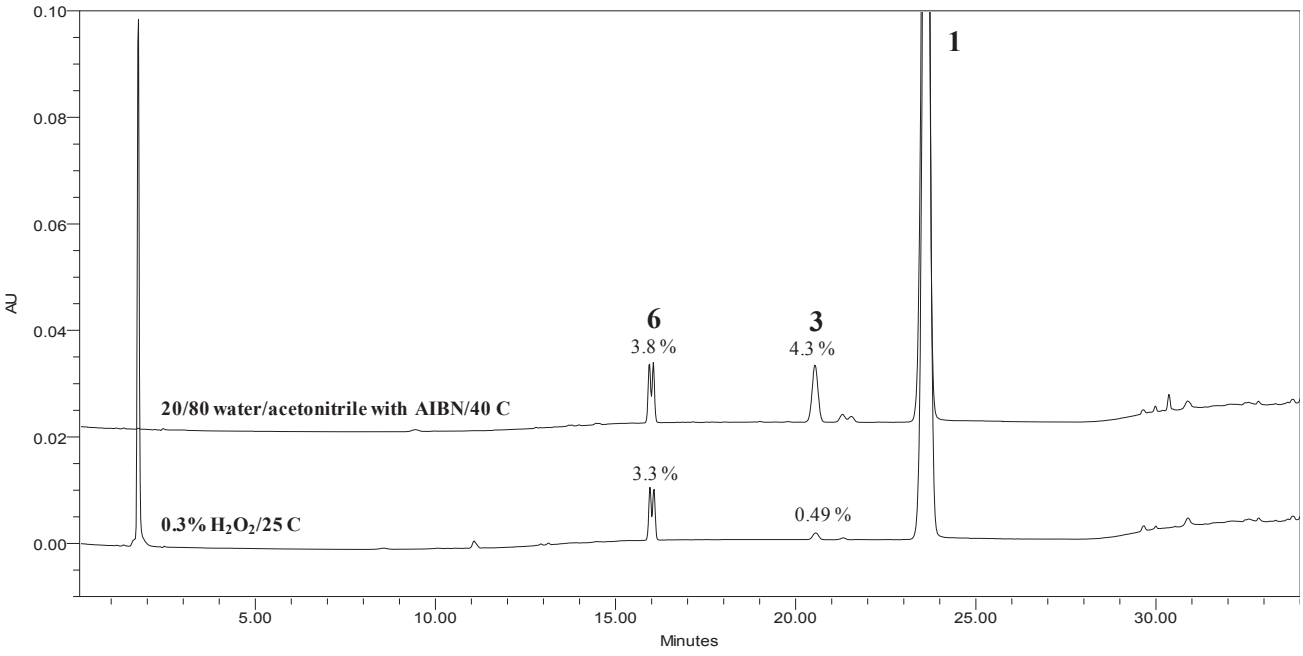

Figure 5. HPLC chromatograms obtained on solutions of **1** stressed under oxidative conditions for 1 day.

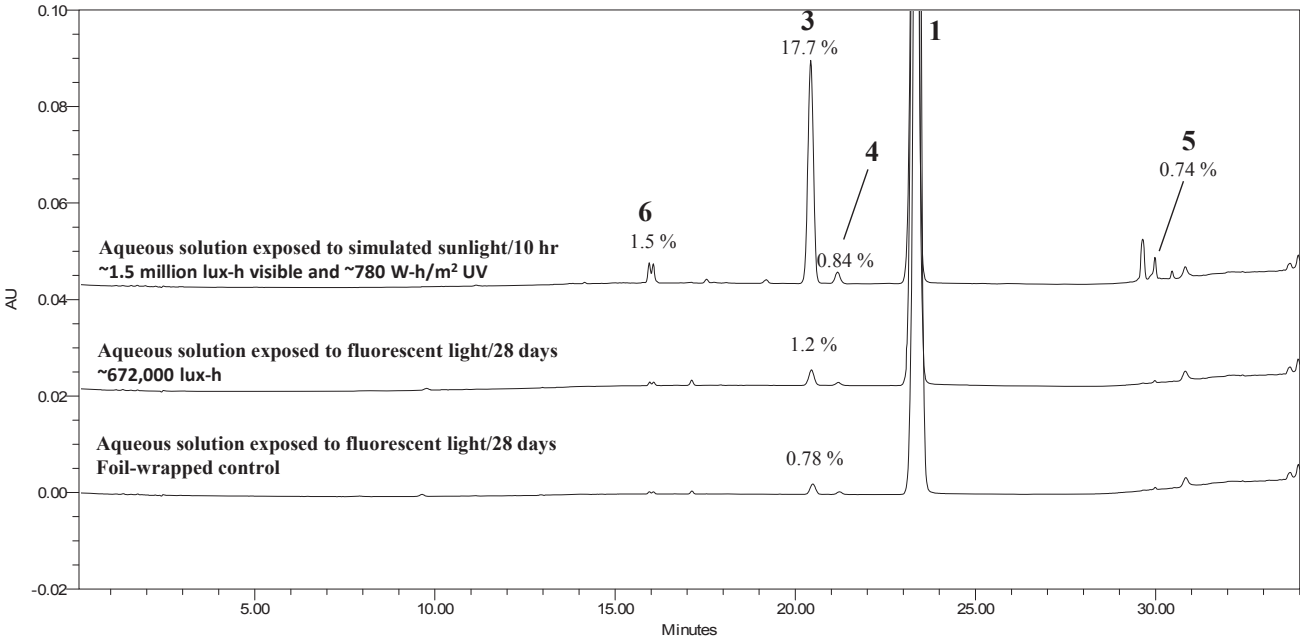

Figure 6. HPLC chromatograms obtained on photostressed solutions of **1**.

(2). One of the key pieces of NMR information used in the determination of the structure is the chemical shift of carbon 24, which at 51.974δ is unusually high field for an oxygenated sp^3-hybridized carbon. Inclusion of this atom in an epoxide substructure explains this unique chemical shift and supports the structure assignment. The proton and carbon chemical data as well as key long-range correlations are given in Table 3.

Oxidative dimers (**3**)—the high-resolution ES^+ measurements on the oxidative dimers (**3**) indicated an *m/z* value of 869.2858 for the protonated molecular ion (Table 4). This mass corresponds to a formula of $C_{40}H_{41}N_{10}O_{13}$ (theoretical mass 869.2849, 0.7 ppm error) and indicates a molecular formula of $C_{40}H_{40}N_{10}O_{13}$ for **3**. This corresponds to the sum of 2 molecules of **1** plus 1 oxygen atom and less than 2 hydrogen atoms. The number of resonances in the carbon NMR spectrum shows that this dimer is not symmetrical. The similarities in the spectra of the 2 benzamidoglutamate moieties indicate that the structures of the 2 halves of the dimer must differ in the heterocyclic portion of the molecule. The presence of a carbonyl resonance at 179.46δ indicates the presence of a lactam similar to the lactam in **6**. This resonance, representing carbon 17 of the oxo half (lower half of dimer as drawn) of the molecule, is long range correlated to overlapping methylene proton resonances at about 2.55δ, thereby identifying the resonances of site 15 of the oxo half of the molecule. Also showing long-range correlations to these protons are quaternary carbon resonances at 144.94, 92.46, and 51.69δ, allowing assignments of these resonances to carbons 11, 24, and 16, respectively, of the oxo half (upper half of dimer as drawn) of the molecule. The assignment of the resonance of carbon 16 is confirmed by its long-range correlation to the protons of methylene 14. The resonances of the exchangeable protons of the heterocyclic system cannot be specifically assigned, but they are similar to analogous shifts in lactams (6). The fact that carbon 16 is quaternary shows that this must be the site of attachment to the other half of the molecule. The chemical shifts of the "ene half" (upper half of dimer as drawn) peaks are similar to those in the spectra of **1**, indicating that the 16-17 double bond is present in this half of the molecule. The long-range couplings were used to aid in the assignments of the resonances of carbons 11', 16', 17', and 24' in this half of the molecule. Again, the resonances of the exchangeable proton occur at expected positions for these compounds. Since the resonance assigned to carbon 17' is that of a quaternary site, it must be the point of attachment to the other half of the molecule.

Ring-opened ketoamine (**4**)—the high-resolution ES^+ measurements on the ring-opened ketoamine (**4**) indicated an *m/z* value of 432.1518 for the protonated molecular ion. This mass corresponds to a formula of $C_{19}H_{22}N_5O_7$ (theoretical mass 432.1514, 1.1 ppm error) and indicates a molecular formula of $C_{19}H_{21}N_5O_7$ for **4**. This formula corresponds to the loss of an oxygen atom and a carbon atom from **1**. Evident in the ^{13}C NMR spectrum is a peak at 197.04δ, which is typical of conjugated ketones. It is therefore proposed that this compound results from an oxidative degradation analogous to that which converts tryptophan to kynurenine.[8,9] This compound has also been determined to be a metabolite of **1**.[10] Additional evidence supporting the assigned structure of **4** is the observation that it is formed over time in acidic solutions of **5.**

Ring-opened ketoformamide (**5**)—the high-resolution ES^+ measurements on the ring-opened ketoformamide (**5**) indicated an *m/z* value of 460.1470 for the protonated molecular ion. This mass corresponds to a formula of $C_{20}H_{22}N_5O_8$ (theoretical mass 460.1463, 1.5 ppm error) and indicates a molecular formula of $C_{20}H_{21}N_5O_8$ for **5**. This formula corresponds to the addition of 2 oxygen atoms to **1**. The ring-opened ketoformamide **(5)** is relatively stable in dilute acidic solution at ambient conditions but degrades with the loss of 28 mass units (CO) to ring-opened ketoamine **(4)** upon heating. Examination of the proton NMR spectrum indicates that the glutamic acid, *p*-disubstituted benzene, and ethylene fragments are still present. The final spin system detected by the correlation spectroscopy experiment involves an exchangeable proton doublet (12.436δ) and a methine (9.418δ). More insight into the nature of this methine can be garnered from the carbon NMR data, which show the chemical shift of this carbon to be 162.566δ, indicating that it is a carbonyl. These results confirm the presence of a formamide. The sharpness of the NH resonance of this substructure is consistent with its being intramolecularly H bonded, presumably to the C16 ketone. Finally, all heteronuclear multiple bond correlation results are in complete accord with the proposed structure of the ring-opened ketoformamide **(5)**.

Table 3
NMR Chemical Shift Assignments for **2**, **4**, **5**, **6**, and **8**

Site	**2**			**4**			**5**			**6**			**8**		
	δH	δC	LRC[a]	δH	δC	LRC[a]	δH	δC	LRC[a]	δH	δC	LRC[a]	δH	δC	LRC[a]
1		173.91	2		173.90	2, 3		173.85	2, 3		173.94	2		183.74, 183.45	2
2	2.35	30.46		2.36	30.40	3, 4	2.35	30.39	3	2.36	30.44	4	2.43	36.06, 35.88	
3	2.07, 1.95	25.98	2	2.07, 1.95	25.90	2, 4, 6	2.09, 1.95	25.93	4, 2	2.0, 1.9	25.93	2,4	2.24, 2.10	30.71, 30.69	2, 4
4	4.38	51.95	2, 3	4.38	51.88	2, 3, 6	4.39	51.88	6, 2, 3	4.39	51.92	2	4.40	58.53, 58.43	2, 3
5		173.52	4		173.5	4		173.43	3		173.53	4		181.54, 181.43	3, 4
6	8.52			8.52			8.50			8.6					
7		166.35	6, (9, 13)		166.67	6, (9, 13)		166.45			166.50	6, (9, 13)		172.60, 172.43	(9, 13)
8		131.81	(10, 12)		131.32	(10, 12)		131.49	(10, 12)		131.52	(10, 12)		133.58, 133.57	(10, 12)
9,13	7.83	127.65	(9, 13)	7.78	127.42	(9, 13)	7.79	127.43	(9, 13)	7.81	127.56	(9, 13)	7.62	129.71	(9, 13)
10,12	7.34	128.06	(10, 12), 14	7.32	128.2	(10, 12), 14	7.33	128.20	(10, 12), 14	7.27	128.25	14	7.14	131.12, 131.09	(10, 12)
11		144.86	(9, 13), 14, 15		146.26	(9, 13), 14,15		145.64	(9, 13), 15, 14		145.59	(9, 13), 14		147.66, 147.60	(9, 13)
14	2.93	31.25	(10, 12), 15	2.85	30.57	(10, 12), 15	2.87	29.97	(10, 12), 15	2.73	31.50	(10, 12)	2.86, 2.34	33.04	(10, 12)
15	2.54	25.26		3.2	44.19	14	3.28	44.53	14	2.06	31.01	14	2.68, 2.31	37.45, 37.35	
16		76.99	14, 15		197.04	14, 15		199.49	15, 14	3.30	43.41	14, 18		79.63	14, 15
17	5.18	80.50	15				9.42	162.57			179.78	16, 18		184.76	15
18							12.44			10.61					
19		174.46	17		154.94	18		155.47			158.03	18		162.10, 162.04	
20															
21		171.02			162.76		12.36 (NH_2)	162.35[b]		6.7 (NH_2)	157.31			160.45, 160.42	
22										10.4					
23		168.40			166.51			162.00[b]			164.60	16, 18		167.25, 167.23	
24		51.97	17		91.95			93.86	18 (NH_2)		90.31	16, 18		95.88, 95.87	

[a] Long-range correlations (LRC)—carbon-proton correlations through 2- and 3-bond coupling. In each cell is a list of the protons which are within 2 or 3 bonds of the carbon in that row.
[b] The resonances of carbons 21 and 23 do not show long-range correlations and may be interchanged.

Lactams (**6**)—the high-resolution ES^+ measurements on the lactams (**6**) indicated an *m/z* value of 444.1515 for the protonated molecular ion. This mass corresponds to a formula of $C_{20}H_{22}N_5O_7$ (theoretical mass 444.1514, 0.2 ppm error) and indicates a molecular formula of $C_{20}H_{21}N_5O_7$ for **6**. This formula corresponds to the addition of a single oxygen atom to **1**. The NMR spectra show no large chemical shift changes in the nuclei of sites 1 through 13, indicating that the oxygen must have been added in the heterocyclic portion of the molecule. The resonances assigned to methylenes 14 and 15 show chemical shift changes, and a new methine proton (H-16, 3.30δ) is coupled to the protons of methylene 15 (2.06δ). In addition, a new carbonyl resonance has appeared at 179.78δ in the ^{13}C NMR spectrum, and the long-range correlations of this resonance indicate that the carbon it represents is within 3 bonds of the protons of both H-16 and H-18. The NMR experiments indicate that the heterocyclic system has undergone oxidation to a lactam.

α-Hydroxy lactams (**8**)—the high-resolution ES^+ measurements on the α-hydroxy lactams (**8**) indicated an *m/z* value of 460.1465 for the protonated molecular ion. This mass corresponds to a formula of $C_{20}H_{22}N_5O_8$ (theoretical mass 460.1463, 0.5 ppm error) and indicates a molecular formula of $C_{20}H_{21}N_5O_8$ for **8**. This formula corresponds to the addition of 2 oxygen atoms to **1**. The NMR spectra of the α-hydroxy lactams **(8)** were measured in D_2O and show many effects of diastereoisomerism; for example, nearly all the resonances of the ^{13}C NMR spectrum are doubled. The proton NMR spectrum shows that substitution in the aromatic ring has not been altered. From the distortionless enhancement of polarization transfer 135 spectrum of the α-hydroxy lactams **(8)** it can be deduced that the structure includes 4 methylenes. In addition, the distortionless enhancement of polarization transfer and the heteronuclear long-range correlation data confirm that the C4 methine is still present and its chemical shift similar to that of the lactams **(6)**. On the other hand, the C16 methine resonance present in the lactams **(6)** is missing from the proton spectrum and the carbon chemical shift of C16 has shifted downfield to 79.63 ppm and is long range correlated to the protons of both methylene groups 14 and 15. On these bases, the diasteromeric α-hydroxy lactam structures are proposed.

Proposed Degradation Mechanisms

The structures of the degradation products and their proposed pathways indicate that **1** degrades via 2 main pathways: oxidation and hydrolysis. Of the 8 identified degradation products (diastereomeric pairs counted as 1 degradation product), 7 (**2**-**6**, **8**, and **9**) are proposed to result from oxidation and 1 (**7**) from hydrolysis. The proposed degradation pathways of **1** are shown in Schemes 1, 2, 3, and 4. The hydrolytic pathway (acidic conditions) **1** is given in Scheme 1. The des-glutamate **(7)** and glutamic acid result from the acid-catalyzed hydrolysis of the amide linkage of **1**. In the stress-testing studies, des-glutamate **(7)** was observed only in solutions at low pH.

The oxidative degradation products (5 of which are also observed upon exposure to light) are proposed to arise through the enolic form of the deazaguanine ring, since aromatic hydroxyls/phenols are known to be highly susceptible to autoxidation via radical mechanisms, especially in the deprotonated/anionic form[11] (Scheme 1). The resulting radical can be extensively delocalized; reaction of molecular oxygen at carbon-17 (per the numbering scheme shown in the structures; Fig. 7) results in hydroperoxide (a); although no direct evidence was obtained for the formation of (a), it is proposed as the common intermediate for all of the oxidative degradation products (Scheme 2). Hydroperoxide (a) is expected to be unstable and is proposed to breakdown via 4 distinct pathways, illustrated by pathways A-D.

Table 4
NMR Chemical Shift Assignments for **3**

Site "Oxo Half"	δH	δC	LRC	Site "Ene Half"	δH	δC	LRC
1		173.92, 173.94		1'		173.92, 173.94	
2	2.30	30.43		2'	2.30	30.43	
3	1.97	25.93, 25.95		3'	1.97	25.93, 25.95	
4	4.30	51.92, 51.91		4'	4.30	51.92, 51.91	
5		173.55, 173.54		5'		173.55, 173.54	
6	8.25			6'	8.25		
7		166.42, 166.61		7'		166.42, 166.61	
8		131.41, 131.50		8'		131.41, 131.50	
9,13	7.76	127.46, 127.56		9', 13'	7.76	127.46, 127.56	
10,12	7.28	127.95, 128.08		10', 12'	7.28	127.95, 128.08	
11		144.94	14,15	11'		146.37	(14', 15')
14	2.45	29.80	(10,12),15	14'	2.55	37.72	(10', 12'), 15'
15	2.55	34.45	14	15'	2.65	27.96	14'
16		51.69	14,15	16'		114.60	(14', 15')
17		179.46	15	17'		123.40	(14', 15')
18	10.95			18'	10.93		
19		158.5		19'		157.69	
20				20'			
21	6.94 (NH_2)	157.80		21'	6.48 (NH_2)	151.75	
22	10.63			22'	10.49		
23		164.10		23'		158.4	
24		92.46	15	24'		99.52	(14', 15')

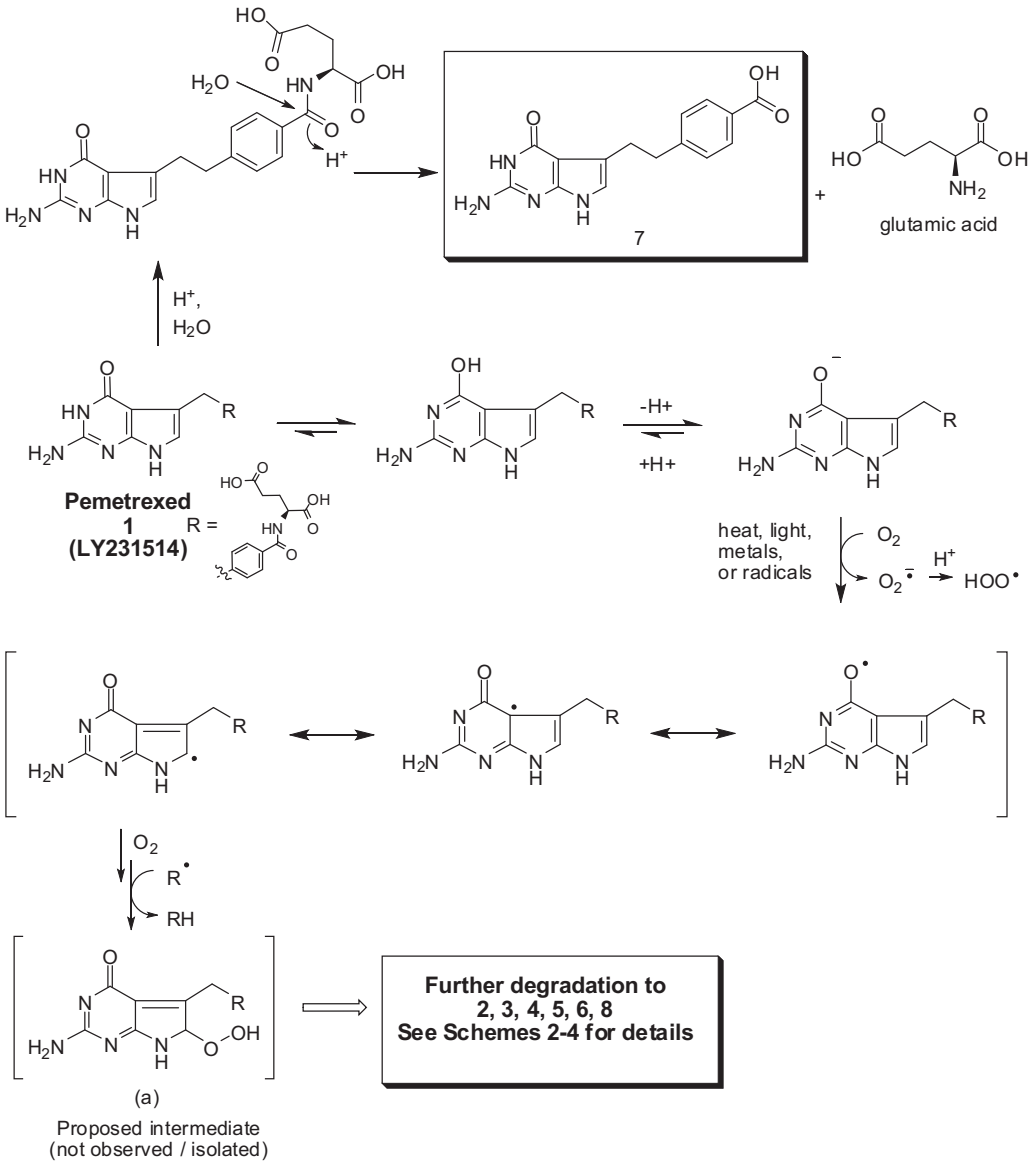

Scheme 1. Proposed degradation pathways of pemetrexed.

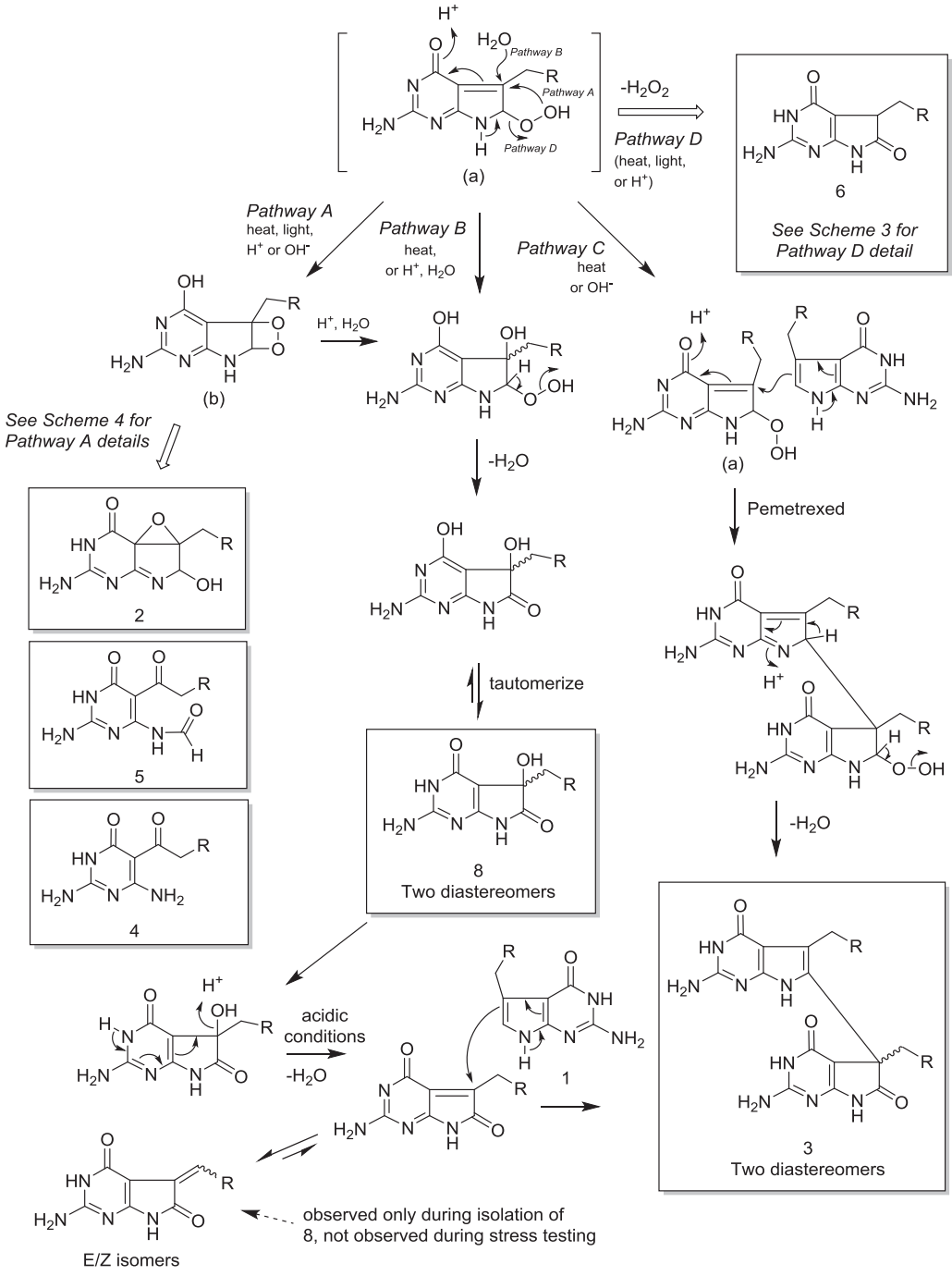

Scheme 2. Degradation pathways of intermediate (a).

Pathway A (Schemes 2 and 4) involves ring closure of the hydroperoxide to dioxetane (b) in the solid state and in solutions across a broad pH range; in the presence of light, dioxetane (b) forms directly from pemetrexed via a (2 + 2) cycloaddition of oxygen (see Discussion section). Dioxetane (b) can give rise to products **2**, **5**, **4**, and **8**. The details of pathway A, which gives rise to products 2, 5, and 4, are shown in Scheme 4. The formation of epoxy hemiaminal (**2**) is particularly noteworthy, as this structure represents a novel degradation pathway of dioxetanes of related ring structures (e.g., indoles, tryptophan, deazaguanines). Degradation product **5** arises from scission of the pyrrolo-dioxetane ring of (b), and subsequent hydrolysis of **5** gives rise to **4** plus formic acid. The formation of **4** from **5** was confirmed by experiment under acidic conditions. As discussed in the Experimental section, this oxidative degradation pathway is analogous to the oxidation of tryptophan to kynurenine.[8,9] The formation of **5** and **4** from dioxetane (**b**) is supported by the observation that solutions of **1** containing the singlet oxygen sensitizer rose bengal undergo rapid degradation to **5** as well as the oxidative dimers (**3**), α-hydroxy lactams **(8)**, and epoxy hemiaminal **(2)** when exposed to light. This type of photo-oxidative degradation is similar to that of indoles, which has been studied extensively.[12]

Pathway B (Scheme 2) involves reaction of hydroperoxide (a) with water under acidic conditions via a 1,4-Michael addition

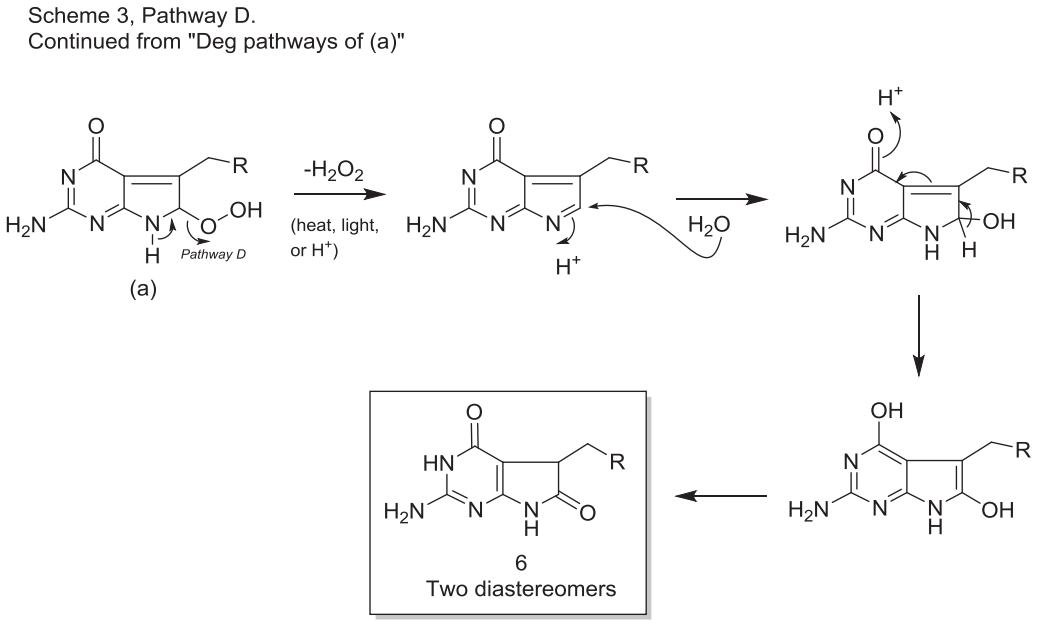

Scheme 3. Formation of 6 (pathway D, continued from Scheme 2).

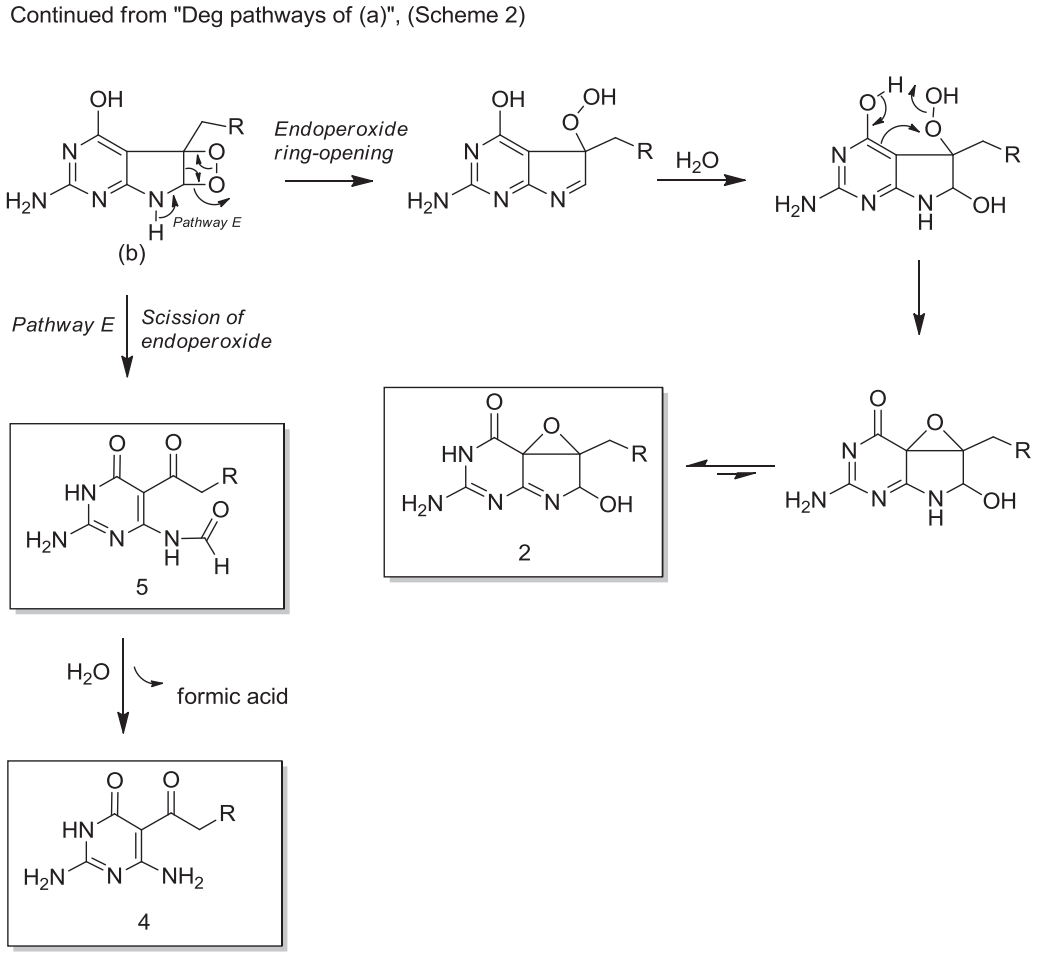

Scheme 4. Formation of 2, 5, and 4 (pathway A, continued from Scheme 2).

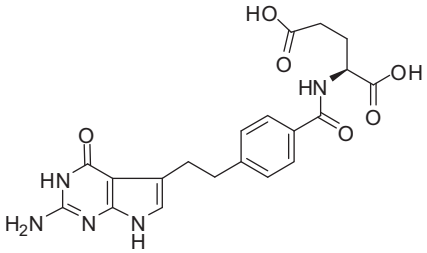

LY231514 (**1**)

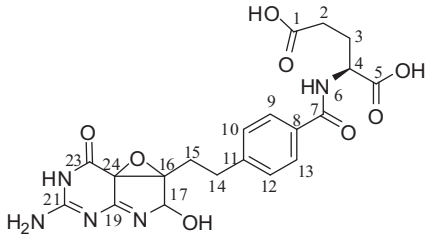

epoxy hemiaminal (**2**)
LSN493331

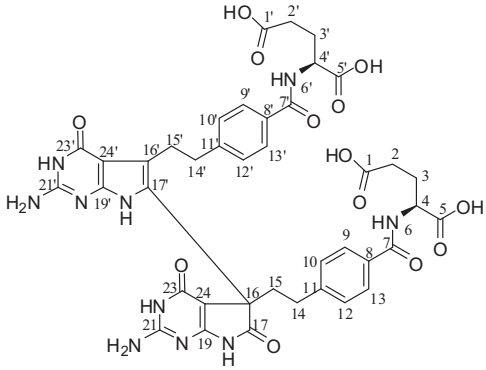

oxidative dimers (**3**)
LSN400075

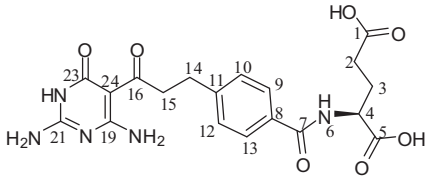

ring-opened keto-amine (**4**)
LSN368962

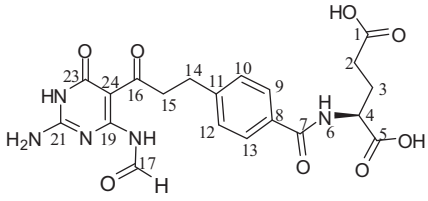

ring-opened keto-formamide (**5**)
LSN472702

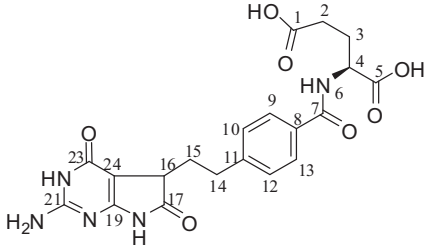

lactams (**6**)
LSN338979

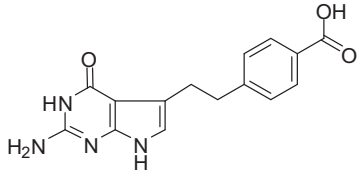

des-glutamate (**7**)
LSN202723

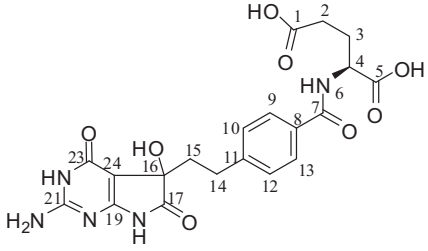

α-hydroxy lactams (**8**)
LSN404452

Figure 7. All structures are shown.

followed by dehydration of the resulting hydroperoxide to form α-hydroxy lactams **8** (during isolation of **8**, dehydration to the E/Z enones was also observed). The potential for **8** to react with pemetrexed (**1**) to form oxidative dimers **3** was tested. Pemetrexed was added to an acidic solution (0.5% HOAc, pH 3.1) of the α-hydroxy lactams **(8)** and heated at 70°C for 40 min. HPLC

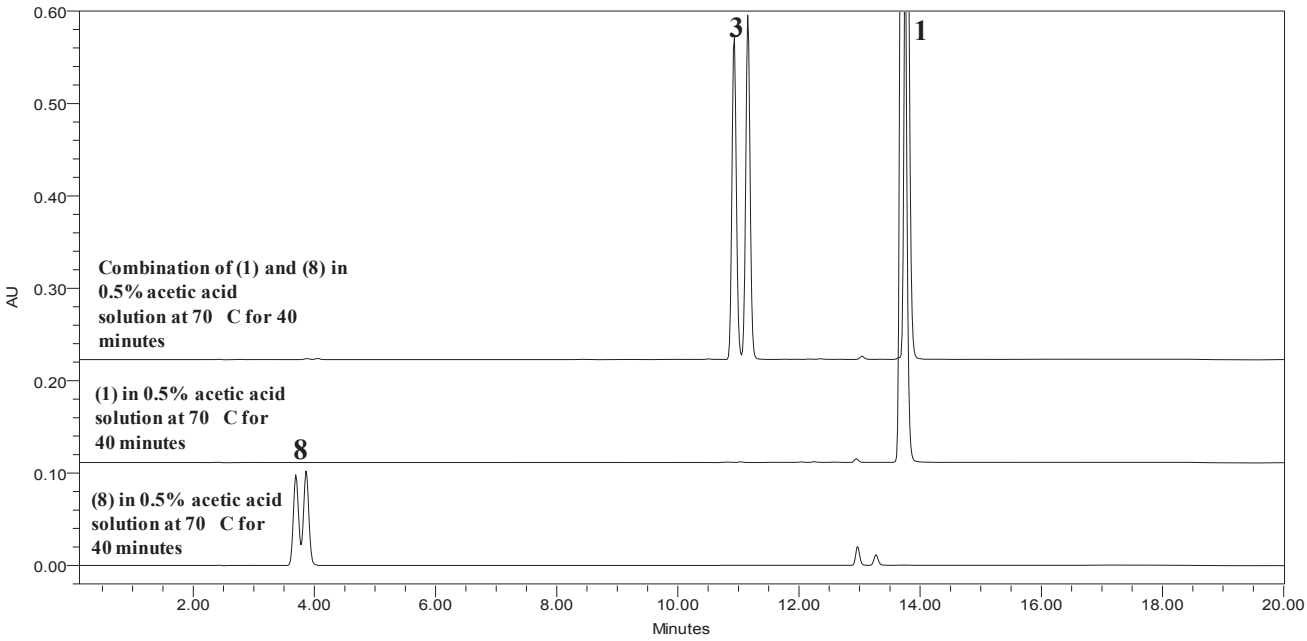

Figure 8. HPLC chromatograms obtained on individual solutions of **8** and **1** and a combination of **8** and **1** together in 0.5% acetic acid heated at 70°C for 40 min. The chromatograms illustrate the reaction of **8** with **1** to give **3**.

analysis of this solution and control solutions of **1** and **8** (Fig. 8) indicated that the α-hydroxy lactams **(8)** do indeed react with **1** to give the oxidative dimers (**3**), confirming that the pathway is a potential route to the oxidative dimers (**3**) at low pH.

Pathway C (Scheme 2) involves reaction of hydroperoxide (a) with pemetrexed (**1**) in the solid state or under basic conditions in solution. Hydroperoxide (a) reacts with **1** via a 1,4-Michael addition to form a dimeric hydroperoxide structure, that upon dehydration yields oxidative dimers **3**.

Pathway D (Scheme 3) represents the fourth degradation pathway of hydroperoxide (a), and this pathway is active in the solid state or in the presence of light or acid in solution. Pathway D involves loss of hydrogen peroxide, followed by addition of water and tautomerization to give lactams **6**. An alternative radical mechanism involving homolytic cleavage of the hydroperoxide (not shown) can also be envisioned. The alkoxy radical formed could then abstract a hydrogen atom to directly give the hemiaminal shown in Scheme 3.

Conclusions

Stress-testing studies have been conducted on **1** drug substance in order to establish its degradation pathway(s). A total of 7 major degradation products detected in the stress-testing studies have been structurally characterized. The structures of the degradation products and their proposed mechanisms of formation indicate that **1** degrades *via* 2 main pathways: oxidation (which can be catalyzed by peroxide, free radicals, or light) and hydrolysis at low pH values. Of the 7 identified degradation products, 6 are proposed to result from oxidation and 1 from hydrolysis. These degradation products have been used to develop stability indicating methods for both the drug substance as well as formulations of **1**. Stability studies conducted on samples of the heptahydrate form of **1** indicate that it is stable and does not undergo degradation when packaged appropriately. Stability studies conducted on the lyophilized formulation of **1** also indicate that it is stable when packaged in vials with a nitrogen overlay to minimize the level of oxygen.

References

1. Saravanan G, Suryanarayanal MV, Jadhav MJ, Ravikumar M, Someswararao N, Acharyulu PVR. A stability-indicating LC assay method for pemetrexed disodium. *Chromatographia*. 2007;66:431-434.
2. Patel AD, Sen DJ, Patel CN. Stability indicating high performance thin layer chromatographic method for estimation of pemetrexed disodium in bulk drug. *Int J Pharm Sci*. 2011;3(2):1208-1214.
3. Patel AD, Parikh SK, Sen DJ, Patel CN. Development and validation of high performance liquid chromatographic and UV spectrophotometric method for estimation of pemetrexed disodium in bulk drug and pharmaceutical formulation. *Int J Drug Dev Res*. 2011;3(2):301-307.
4. Meera N, Mankumare SD, Adyanth K, Chakravarthy T, Wadekar KR, Ravi P. Determination of related substances in pemetrexed disodium (form IV) in bulk drug samples by HPLC. *Pharm Technol*. 2014;38(2).
5. Respaud R, Tournamille JF, Croixa C, Laboriea H, Elfakir C, Viaud-Massuarda MC. Development of an ion-pairing reversed-phase liquid chromatography method using a double detection analysis (UV and evaporative light scattering detection) to monitor the stability of Alimta®-pemetrexed preparations: identification and quantification of l-glutamic acid as a potential degradation product. *J Pharm Biomed Anal*. 2011;54:411-416.
6. Warner* A, Piraner I, Weimer H, White K. Development of a purity control strategy for pemetrexed disodium and validation of associated analytical methodology. *J Pharm Biomed Anal*. 2015;105:46-54.
7. International Council for Harmonization Q1A (R2), stability testing of new drug substances and products, 2000; ICH Q1B, Photostability Testing of New Drug Substances and Drug Products, 1996.
8. Adam W, Ahrweiler M, Sauter M, Schmiedeskamp B. Oxidation of indoles by singlet oxygen and dimethyldioxirane: isolation of indole dioxetanes and epoxides by stabilization through nitrogen acylation. *Tetrahedron Lett*. 1993;34(33):5247-5250.
9. Graziella E, Ronsein MCBO, Miyamoto S, Medeiros MHG, Mascio APD. Tryptophan oxidation by singlet molecular oxygen [O2 (1Δg)]: mechanistic studies using 18O-labeled hydroperoxides, mass spectrometry, and light emission measurements. *Chem Res Toxicol*. 2008;21:1271-1283.
10. Woodland JM, Barnett CJ, Dorman DE, et al. Metabolism and disposition of the antifolate LY231514 in mice and dogs. *Drug Metab Dispos*. 1997;25(6):693-700.
11. Baertschi SW, Alsante KM, Santafianos D. Stress testing: the chemistry of drug degradation. In: Baertschi SW, Alsante KM, Reed RA, eds. *Pharmaceutical Stress Testing: Predicting Drug Degradation*. 2nd ed. New York: Informa Healthcare; 2011:99-100.
12. Saito I, Matsugo S, Matsuura T. Mechanism of indole-singlet oxygen reactions. Interception of zwitterionic intermediates. *J Am Chem Soc*. 1979;101:7332.